New Findings of the Sporadic E (Es) Layer Development Around the Magnetic Equator During a High-Speed Solar (HSS) Wind Stream Event

L. C. A. Resende[1,2] ⓘ, Y. Zhu[1], C. M. Denardini[2] ⓘ, I. S. Batista[2] ⓘ, J. Shi[1] ⓘ, J. Moro[1,3] ⓘ, S. S. Chen[2] ⓘ, F. Conceição-Santos[4,5], L. A. Da Silva[1,2] ⓘ, V. F. Andrioli[1,2] ⓘ, M. T. A. H. Muella[4] ⓘ, P. R. Fagundes[4] ⓘ, A. J. Carrasco[6] ⓘ, V. G. Pillat[4] ⓘ, C. Wang[1] ⓘ, and Z. Liu[1]

[1]State Key Laboratory of Space Weather, Beijing, China, [2]National Institute for Space Research — INPE, São José dos Campos, Brazil, [3]Southern Space Coordination — COESUL, Santa Maria, Brazil, [4]Universidade do Vale do Paraíba-UNIVAP, Instituto de Pesquisa e Desenvolvimento-IP&D, Lab. de Física e Astronomia, São José dos Campos, Brazil, [5]Instituto Federal de Educação Ciência e Tecnologia do Maranhão — IFMA, Açailandia, Brazil, [6]Universidade de Los Andes, Mérida, Venezuela

Abstract The equatorial (Es_q) and blanketing (Es_b) sporadic (Es) layers occur due to the Equatorial Electrojet Current (EEJ) plasma instabilities and tidal wind components, respectively. Both Es_q and Es_b layers can appear concurrently over some Brazilian equatorial regions due to the peculiar geomagnetic field configuration in this sector. Previous works indicate that the inclination angle limit for the Es_q occurrence in ionograms is 7°. However, we found evidence that regions more distant can also experience such equatorial dynamics during disturbed periods. In this context, we deeply investigated this EEJ influence expansion effect by analyzing the Es_q layers in regions not so close to the magnetic equator during a high-speed solar wind stream event that occurred on May 05 and 06, 2018. To explain these atypical Es_q layer occurrences, we considered the Es layer parameters obtained from digital ionosondes over the Brazilian regions, São Luís (dip: 9.5°), and Araguatins (dip: 10.5°). We use magnetometer data and a model named MIRE (E Region Ionospheric Model) to validate this mechanism. The results show that the eastward electric field of the Gradient Drift instability in the EEJ is effective during the magnetic storm main phase in the boundary equatorial magnetic sites, creating the Es_q layers. Thus, the EEJ plasma irregularity superimposes the wind shear mechanism, changing the Es layer dynamics during disturbed periods over the magnetic equator boundary sites. Therefore, this work establishes new findings of the EEJ influence expansion dynamics in the Es layer formation over the Brazilian regions, which was considered in MIRE for the first time.

1. Introduction

The eastward electric current during the daytime driven by the zonal and vertical electric fields is named Equatorial Electrojet (EEJ) (Forbes, 1981; Moro et al., 2016a, 2016b). This current is caused by the upward vertical polarization electric field, which drives an additional Hall current superimposed to the Pedersen current. The EEJ occurs at the magnetic equator region around 95–115 km of altitude due to the high E region conductivity (Denardini et al., 2004, 2005).

The EEJ is associated with the electron density gradient, and it produces plasma instabilities in the E region. The Gradient Drift instabilities (or Type II irregularities) in the EEJ are generally observed in the 50 MHz backscatter coherent radar data as fluctuations in the Doppler shifts (Denardini et al., 2004), and in ionograms as type "q" sporadic E-layers (Es) (Es_q) (Rastogi, 1972; Resende et al., 2013; Moro et al., 2017). The Es_q layer concept is different from the blanketing Es layers (Es_b) since they do not produce electron density enhancements (Piggott & Rawer, 1972). These layers are observed as diffuse and non-blanketing traces in ionograms. It means that they do not block the radio signal propagation to the upper regions as the Es_b layers. The latter are characterized as denser and thin layers, mainly formed by the wind shear mechanism or particle precipitation (Abdu & Batista, 1977; Haldoupis, 2011; Mathews, 1998; Whitehead, 1961, 1989). However, both Es layer modalities occur in the E region around 90–130 km of altitude, and they could be

considered permanent layers due to their frequent observation and the long metallic ions lifetime, such as Fe^+, Mg^+, K^+, Ca^+, and Na^+ (Kopp, 1997).

Some authors have widely studied the competition between the Es_q and Es_b layers. Knecht and McDuffie (1962) showed that the Es_q signature appears in ionograms as a radio signal scattering covering most frequencies during the daytime since the EEJ plasma irregularities are stronger, and it is not possible to occur Es_b in this period. Nevertheless, Rastogi (1972) showed a strong relationship between the Es_q layers and the eastward electric field. In these cases, if the electric field component weakens, Es_b layers can be formed. Based on this statement, Devasia et al. (2004) using VHF backscatter radar, digital ionosonde, and ground-based magnetometer data from Trivandrum, India (8.5°N, 77°E, dip: −0.5) concluded that the Es_q layer disappearance was associated with the electrojet current reversal (Counter Equatorial Electrojet, CEJ). They affirmed that the vertical polarization electric field reversed to downward (negative) during CEJ events, and the Type II irregularities were too weak to sustain the instabilities. During those events the Es_b layers were frequently recorded in the ionograms at Trivandrum. For the same station, Devasia et al. (2006) analyzed the Es_b layer characteristics during the summer solstice months between 1986 and 2000. Their results confirmed that the majority of the Es_b layer cases are associated with CEJ events. The authors attributed the Es_b layer development in equatorial regions to wind action. In this case, the wind acts in the EEJ irregularity dynamics, generating large vertical polarization electric fields leading to ionization convergence. This is the most acceptable explanation for those occurrences since the wind shear mechanism is not effective at regions located very close to the magnetic equa. In the equatorial regions, as the vertical component of the magnetic field lines is null, and the electrons follow the magnetic field lines, it is not possible that dense Es (Es_b) layers due to the windshear mechanism can form (Abdu et al., 1997; Resende et al., 2016). In other words, in equatorial regions the Es_b layer is not generated by the wind shear process but is due to other formation mechanisms.

During the disturbed periods, Rastogi (1997) studied the Es_q behavior over stations in India using 20 years of ionospheric data. They found an evident Es_q disruption during the main phase of magnetic storms when a decrease of the geomagnetic field H component is noticed in magnetic data. They associated this relationship with the temporary occurrence of the westward electric field over the equatorial ionosphere. Their results show that this westward electric field was strong enough to temporarily reverse the normally eastward electric field in the dayside ionosphere. Thus, the EEJ weakens, and consequently, the Es_q layers disappear. Denardini et al. (2016) analyzed the evolution of the density parameters in Es layers during the October 2003 super magnetic storm over a Brazilian equatorial region. They identified peaks in the frequency parameters, which accompanied changes in the Es layer behavior observed by the Digisonde. They assumed that these peaks indicated the Es_b layers presence during the magnetic storm recovery phase, and they are correlated with the CEJ occurrence.

Over the Brazilian sector, the geomagnetic field configuration has a peculiar behavior. The magnetic inclination angle over northeast Brazil varies at a rate of 20′ per year, corresponding to an apparent northwestward movement of the magnetic equator at a rate of 11.6′/year (Batista et al., 2011). Abdu et al. (1997) analyzed 16 years of ionosonde data over Fortaleza, Brazil (3.8°S, 38°W, dip: −1.7° to −11°). Their results showed that the Es_b layers became more frequent as the magnetic equator departs from that station. They attributed these Es_b layers to the wind shear mechanism. Resende et al. (2013) performed a similar study over São Luís, Brazil (2.53°S, 44.25°W, dip: −1.9° to −3.8°) during the solar cycle 23 when the magnetic equator was located around this region. They found similar results, in which the Es_b layers occurrence increases with the magnetic equator displacement. Thus, the authors confirm that in some regions over the Brazilian sector, named "transition regions," it is possible to simultaneously observe the Es_q and Es_b layers.

More recently, Resende et al. (2016) analyzed the competition between winds and electric fields in the Es_b formation over São Luís using observational data and simulations. They verified that the Es_b layers appeared during some hours when the EEJ irregularity was weak, which means that the wind shear mechanism has been effective. Moro et al. (2017) simulated the zonal and vertical electric fields of the EEJ instabilities and analyzed the Es layer formation over São Luís during the November 2004 geomagnetic storm. Their analysis confirms that the electric field components are the main agent responsible for the Es_q occurrences, and consequently, the Es_b layer disruption.
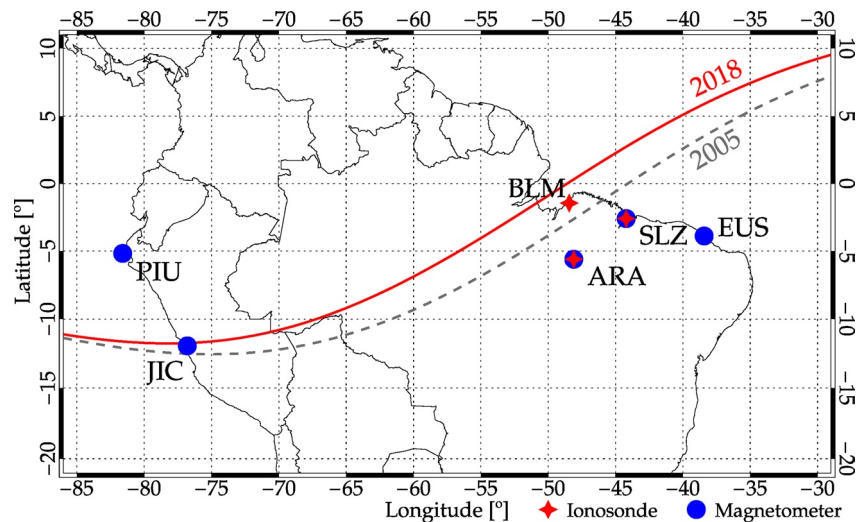
Figure 1. Map showing the instrument sites used in this study. The magnetic equator positions in 2018 (red line) and 2005 (gray dashed line) are also shown. The acronyms identify the following stations: BLM is Belém, SLZ is São Luís, ARA is Araguatins, EUS is Eusébio, JIC is Jicamarca, and PIU is Piura.

The inclination angle limit for the Es_q occurrence in ionograms is not well established yet. Until now, we observe both Es_b and Es_q traces in ionograms in some Brazilian equatorial sectors. Thus, competing mechanisms act in the Es layer formation: wind shear and EEJ irregularities. In previous work, Resende et al. (2021) had the first evidence that it was possible to observe the Es_q layer in a region not so close to the magnetic equator. They proposed that the Es_q layer appearance in ionograms could be triggered during disturbed periods. Specifically, the authors analyzed the zonal westward electric field due to the disturbance dynamo effect, and their results showed a low correlation between this and the Es layer behavior over SLZ. Moreover, they ascribed some unrealistic results given by an E region numerical model (MIRE - Portuguese acronym for E Region Ionospheric Model) to the non-inclusion in the simulations of the EEJ dynamics.

In the present study, we deeply investigated how EEJ affects the Es layer formation considering its physical dynamics. To analyze this behavior, we study the Es layer development at two regions located in the magnetic equator border, SLZ (2.53°S, 44.25°W, dip: −9.5°), and Araguatins (ARA, 5.64°S, 48.11°W, dip: −10.5°). Also, we analyzed one region located at the magnetic equator to try observing these Es layer development, Belém (BLM, 1.45°S, 48.49°W, dip: −2.5°). We performed a case study using a period around the moderate geomagnetic storm of May 2018. The ionosonde and fluxgate magnetometer data were used to prove the occurrence or suppressions of the Es_q and Es_b layers and the related formation mechanisms. We simulated the Es layer for this period through of the MIRE to evaluate the EEJ electric field effects in its development. Finally, this study is a good opportunity to understand the unclear dip equator secular displacement effect in the Es layer formation mechanism.

2. Data Selection and Methodology

In this study, we used data from ionosondes, and magnetometers installed in regions around the magnetic equator to study the formation or disruption of Es_q and Es_b layers in the days before, during, and after the geomagnetic storm that occurred on May 06, 2018. The equipment locations used in this analysis are shown in Figure 1. The magnetic equator position calculated using the International Geomagnetic Reference Field (IGRF) model is shown as the red line for the year 2018 and as the gray dashed line for the year 2005 to illustrate the movement of the magnetic equator. In the following, we briefly describe each set of data used in the present study.

2.1. Ionosonde Data

The digital ionosondes provided the Es parameters in the three analyzed stations. This class of equipment is basically a radar that continuously operates at frequencies ranging from 1 to 20–30 MHz, depending on their type. Here, we used two different digital ionosondes: Lowell Digisonde (Reinisch et al., 2009) to investigate the Es over BLM and SLZ sites, and Canadian Advanced Digital Ionosonde (CADI) (MacDougall et al., 1995) to analyze the same ionospheric parameters over the ARA station. We manually checked the data in both types of equipment since significant discrepancies can be found between the automatically scaled and the correct values in the Brazilian region (Resende et al., 2020). The ionosondes provide the ionospheric profile in graphs of frequency versus virtual height, from which it is possible to obtain the desired parameters.

We used the SAO-Explorer to study the ionospheric layers with the Digisonde. This program contains the Automatic Real-Time Ionogram Scaler (ARTIST) software (Reinisch & Huang, 1983) that allows getting the ionospheric parameters for the F and E regions with Es layers which, for the period analyzed, have a cadence of 10 min. We obtained the following parameters for this work: fbEs (Es layer blanketing frequency), and ftEs (Es layer maximum frequency). Concerning the CADI data, we used a software tool named UDIDA-UNIVAP Digital Ionosonde Data Analysis (Pillat et al., 2013), which facilitates the visualization and analysis of the ionograms, and the ionospheric parameters are recorded every 5 min.

As mentioned before, the Es layers were classified as blanketing-Es_b or equatorial-Es_q layers. The Es_b types are divided in cusp (Es_c), high (Es_h), flat (Es_f), low (Es_l), auroral (Es_a), and slant (Es_s) types, following the International Union of Radio Science (URSI) criterion, which is available in the URSI Handbook of Ionogram Interpretation and Reduction (Piggott & Rawer, 1972). In this study, we use the term Es_b to refer to the Es layers formed by the wind shear mechanism and Es_q to refer to the Es layers created by the EEJ irregularities.

2.2. Magnetometer

We used data from magnetometers installed in the Brazilian and Peruvian sectors, as shown in Figure 1. Two sites are necessary to obtain the EEJ ground strength, one under the dip equator, and another outside of the EEJ influence. Also, we used the 1 min average of the H component measurements from the two sites to determine the magnetic effect of the EEJ strength at the ground level (named EEJ ground strength for simplification).

The magnetic data treatment focus on eliminating outlier values from the measured components based on a third-order polynomial fitting. Then, the five quietest days of the month are chosen, and their local midnight values are averaged ($\langle H_{00} \rangle$). After that, the H component variation is normalized using:

$$\Delta H_{\text{Station}} = H_{\text{Station}} - \langle H_{00} \rangle, \tag{1}$$

which is computed using the difference between the H component and the mean midnight value for each station $\left(\Delta H_{\text{Station}} \right)$. Thus, the EEJ ground strength diurnal variation is estimated by:

$$\Delta H_{\text{EEJ}} = \Delta H_{\text{eq}} - \Delta H_{\text{out}}, \tag{2}$$

in which ΔH_{eq} is the ΔH of a station at the dip equator, and ΔH_{out} is the ΔH of a station outside the EEJ influence. A more detailed explanation of the magnetic data treatment and the use of these two stations is given in Denardini et al. (2009, 2018).

In this study, we evaluate the EEJ current using the magnetometers located in SLZ and ARA (Figure 1). Since the BLM station does not have a magnetometer, we used the Jicamarca (JIC, 11.95°S, 76.88°W, dip: −0.5°) magnetometer data as a proxy because both stations are very near to the magnetic equator line. Thus, it is possible to confirm that SLZ and ARA regions had an equatorial behavior, ensuring that the EEJ influence expansion can still influence these stations. For off equatorial stations in the EEJ ground strength calculation, we used Eusébio (EUS, 3.88°S, 38.42°W, dip: −18.5°) data for Brazilian regions ($\Delta H_{\text{EEJ}} = \Delta H_{\text{SLZ}} - \Delta H_{\text{EUS}}$ or $\Delta H_{\text{EEJ}} = \Delta H_{\text{ARA}} - \Delta H_{\text{EUS}}$) and Piura (PIU, 5.17°S, 80.64°W, dip: −12.1°) for the Peruvian sector ($\Delta H_{\text{EEJ}} = \Delta H_{\text{JIC}} - \Delta H_{\text{PIU}}$).

2.3. Winds and Electric Fields in MIRE Model

A theoretical model, called MIRE, is used to simulate the Es layer dynamics in equatorial and low latitudes over the Brazilian region (Resende et al., 2016, 2017a, 2017b, 2020; Moro et al., 2017). The model provides the E region electron density through the resolution of the continuity and momentum differential equations for the molecular/atomic (NO^+, O_2^+, N_2^+, O^+) and metallic (Fe^+, Mg^+) ions. The equations are solved for a height versus time grid. The height ranges from 86 to 120 km in steps of 0.05 km, whereas the time ranges from 00 LT to 24 LT in steps of 2 min. All the details about this model can be found in Carrasco et al. (2007) and Resende et al. (2017a).

The ions' vertical velocity is obtained using:

$$V_{iz} = \frac{\omega_i^2}{\left(v_{in}^2 + \omega_i^2\right)} \left[\begin{array}{l} \cos I \cdot \sin I \cdot U_x + \frac{v_{in}}{\omega_i} \cdot \cos I \cdot U_y + \frac{1}{v_{in}} \frac{e}{m_i} \cdot \cos I \cdot \sin I \cdot E_x \\ + \frac{e}{\omega_i m_i} \cdot \cos I \cdot E_y + \frac{e}{v_{in} m_i} \cdot \left(\frac{v_{in}^2}{\omega_i^2} + \sin^2 I \right) \cdot E_z \end{array} \right], \tag{3}$$

where ω_i is the ion gyrofrequency, v_{in} is the ion-neutral collision frequency, I is the magnetic inclination angle, m_i is the ion mass, e is the ion electric charge, E_x, E_y, and E_z are the electric field components, and U_x is the meridional and U_y is the zonal wind components. The following reference system represents all the vectors: the X-axis points toward the south, and the Y-axis points to the east, whereas the Z-axis completes the right-handed coordinate system, pointing up.

We used the GSWM-00 model, which successfully describes the wind dynamics near the magnetic equator regions (Buriti et al., 2008; Hagan & Forbes, 2002, 2003). The GSWM-00 can be obtained from the website of the High-Altitude Observatory (HAO) of the National Center for Atmospheric Research (NCAR) in Colorado (http://www.hao.ucar.edu/modeling/gswm/gswm.html). This wind model provides the semidiurnal (12 h), and diurnal (24 h) amplitudes, the phase, and the wavelength for the zonal and meridional tidal wind components over each region analyzed. Afterward, these parameters are included in the following wind shear equations:

$$U_x(z) = U_{x0}(z) \cdot \cos\left(\frac{2\pi}{\lambda_x}(z - z_0) + \frac{2\pi}{T}(t - t_{x0}(z)) \right) \tag{4}$$

$$U_y(z) = -U_{y0}(z) \cdot \sin\left(\frac{2\pi}{\lambda_y}(z - z_0) + \frac{2\pi}{T}(t - t_{y0}(z)) \right). \tag{5}$$

where $U_{x0}(z)$ and $U_{y0}(z)$ correspond to wind amplitudes at the height z, λ_x, and λ_y are the wavelengths, T is the tidal period (24 h for diurnal and 12 h for semidiurnal), z_0 is a reference height, assumed as 100 km, and $t_{x0}(z)$ and $t_{y0}(z)$ are the wave phases.

The E region electric field components are usually studied in terms of the Doppler shifts of Type II echoes detected with coherent and incoherent radars (Devasia et al., 2006; Moro et al., 2017). However, we do not have radar data for the studied periods. Therefore, to obtain the electric field, we used the methodology presented by Anderson et al. (2004). They used a neural network to obtain the following relationship between the vertical drift velocity ($E \times B / B^2$) in the regions near to equator and the ΔH:

$$\begin{aligned} E \times B / B^2 = & -1989.51 + 1.002 \text{year} - 0.00022 \text{DOY} - 0.0222 F10.7 \\ & - 0.0282\, F10.7A - 0.0229 Ap_{\text{daily}} + 0.0589 Kp - 0.3661 \text{LT} \\ & + 0.1865 \Delta H + 0.00028 \Delta H^2 - 0.0000023 \Delta H^3, \end{aligned} \tag{6}$$

where DOY is the day of the year, $F10.7$ is the solar flux measured at the 10.7 cm wavelength, $F10.7A$ is a 3-month average of the $F10.7$ index. The Ap index is based on magnetometer data and provides a daily average level for geomagnetic activity. Therefore, the Ap_{daily} is an average of the 8 daily values of the Ap. The LT is the local time, and the ΔH refers to the ΔH_{EEJ} that depends on the region analyzed. The geomagnetic field intensity is obtained through the IGRF (http://wdc.kugi.kyoto-u.ac.jp/igrf/).
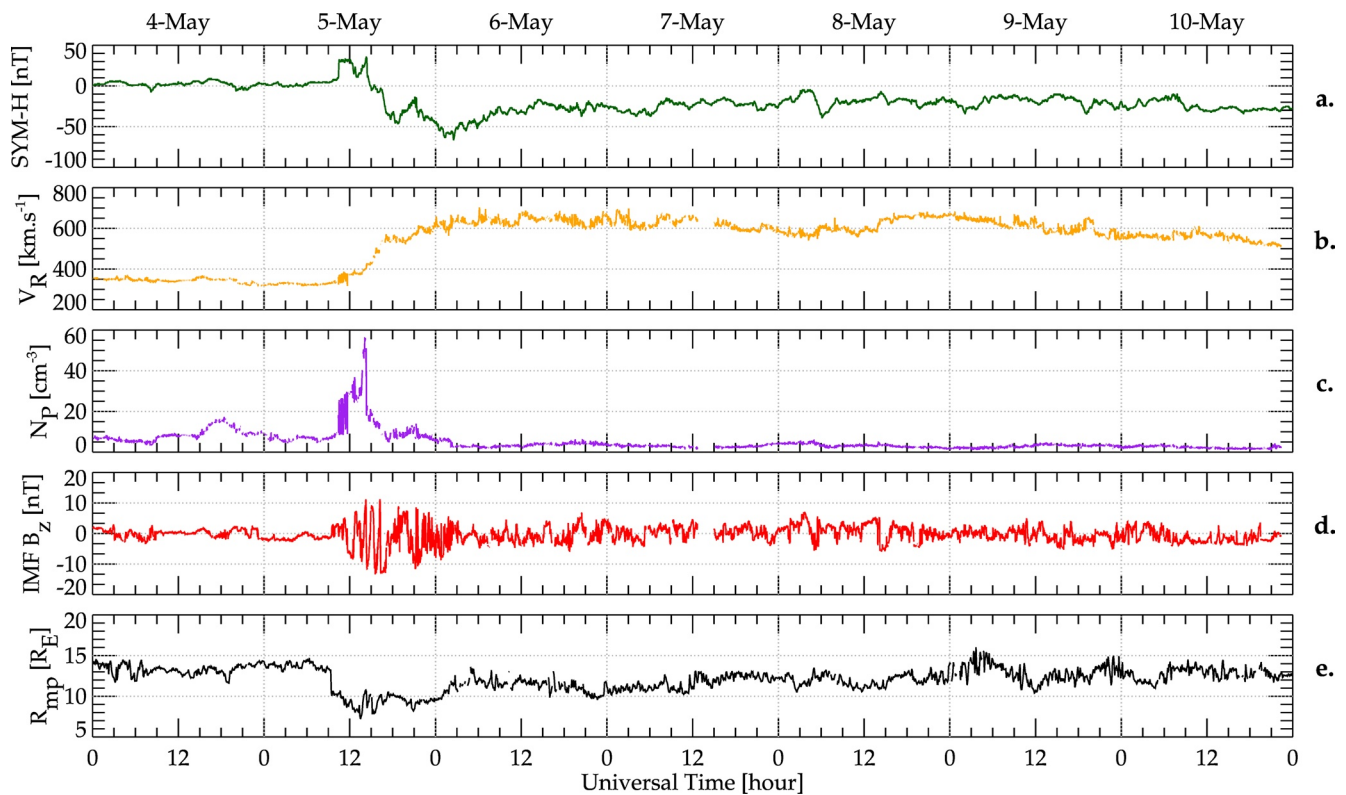
Figure 2. (a) The SYM-H index, (b) the solar wind velocity V_R, (c) the number density of protons N_P, (d) the interplanetary magnetic field component B_z, and (e) the magnetopause standoff distance R_{mp}, from May 04 to 10, 2018.

It is important to mention here that this method was validated for the Brazilian regions (Nogueira et al., 2013) and provides a good estimation of the E layer electric field during the daytime, which is our interest in this study. Thus, the zonal electric field and the wind components are included in Equation 3 to evaluate the Es layer development.

3. Results and Discussions

3.1. Interplanetary Medium Conditions

The study period for the three Brazilian regions located close to the magnetic equator is May 04–10, 2018. The interplanetary medium conditions at the L1 Lagrangian point were embedded by a high-solar wind speed stream (HSS). The interplanetary medium parameters obtained from the Magnetic Field Experiment (MAG) and Proton and Alpha Monitor (SWEPAM) instruments onboard the Advanced Composition Explorer (ACE) spacecraft (Stone et al., 1998) confirmed the passage of the HSS toward Earth's magnetosphere. This solar wind structure reached the Earth's magnetosphere on May 05, 2018, and its effect on the atmosphere lasted at least until May 10, 2018.

Figure 2 shows (a) the variations of the SYM-H index in nT, (b) the solar wind velocity in km/s (V_R), (c) the number density of protons per cm³ (N_P), (d) the interplanetary magnetic field component (IMF) in nT (B_z), and (e) the magnetopause standoff distance (R_{mp}) in R_E (Earth radii). R_{mp} was calculated by an empirical model (Shue et al., 1998), in which the solar wind parameters are used. The solar wind structure reached the L1 Lagrangian point at 0927 UT on May 05, 2018, with a significant solar wind velocity increase from 320 to 600 km/s. Simultaneously, the density increased abruptly, and the B_z component presented significant fluctuations during all day. The SYM-H reached −66 nT on May 06, 2018, characterizing a moderate magnetic storm event. After that, SYM-H started to recover and remained around −30 to −20 nT in the next days.
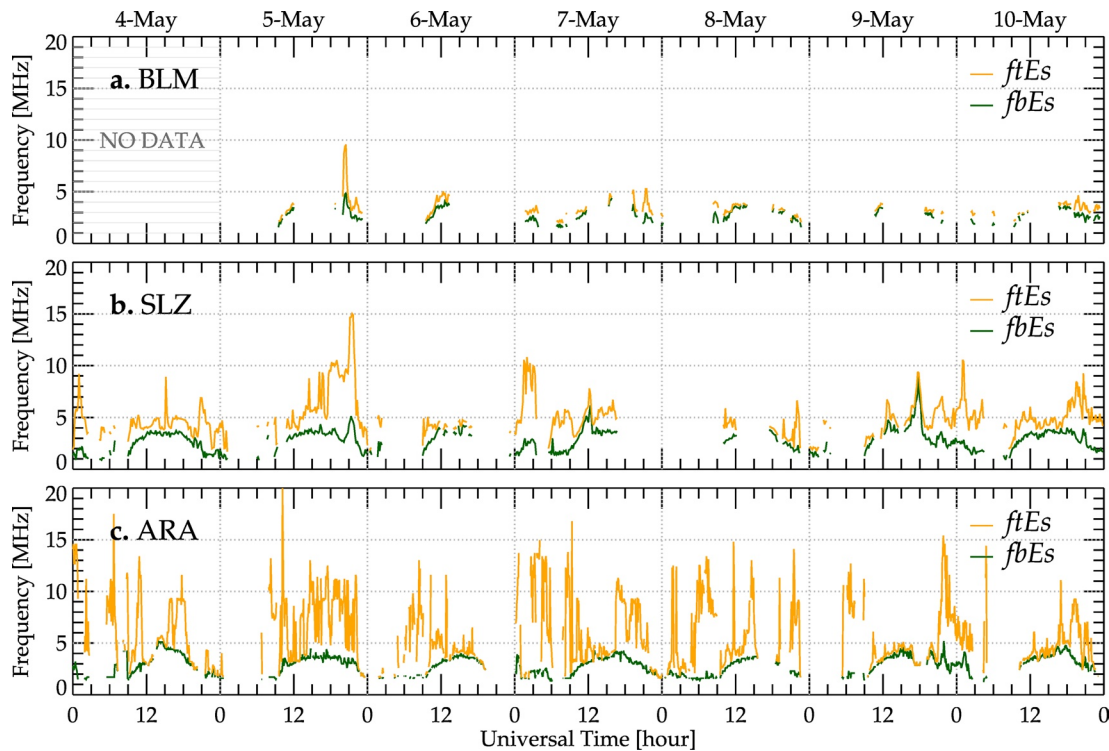
Figure 3. The Es layer blanketing frequency (*fb*Es) (green line) and Es layer maximum frequency (*ft*Es) (orange line) parameters at (a) Belém (BLM), (b) São Luís (SLZ), and (c) Araguatins (ARA) on May 04–10, 2018.

The R_{mp} calculated under the influence of this HSS gives a reasonable estimation of the magnetosphere's compression (Shue et al., 1998), which can be observed in Figure 2e around 1330 UT on May 05, 2018 ($\sim 7\,R_E$). It means that the magnetosphere can have been received a considerable amount of energy (Ponomarev et al., 2006). This energy deposit can cause significant changes in the magnetosphere and consequently impact the ionized and neutral atmosphere. For example, the generation of magnetospheric waves in a wide range of frequencies can directly influence the energy electron flux trapped in the radiation belts (Da Silva et al., 2019, 2021), causing particle precipitation to the atmosphere. The Alfvénic fluctuations observed from May 06 to 10, 2018 (not shown here) are also important to analyze because they indicate that reconnection on the Earth's dayside magnetopause may occur. Consequently, it can cause moderate geomagnetic storms (Gonzalez et al., 1994; Tsurutani et al., 1995) that affect the ionosphere directly.

Hajra et al. (2017) analyzed the ionosphere effects over Arecibo during April 04–08, 2008, also under the influence of an HSS. They observed that the topside ionosphere in this region becomes hotter compared to the quiet periods. The authors credit this behavior to the prompt penetration electric field due to the *B*z fluctuations during this type of solar wind structure. In the E region, Rout et al. (2017) found some results showing that the IMF *B*z predominantly affect EEJ during HSS events on some occasions, intensifying this current system. However, we did not find any work related to the Es layer responses in equatorial regions during the HSS occurrences.

3.2. Sporadic E-Layer Behavior in the Equatorial Region

We analyzed the *fb*Es (green line) and *ft*Es (orange line) parameters over (a) BLM, (b) SLZ, and (c) ARA, as shown in Figure 3. It is well-known in the literature that the Es_q present low values of *fb*Es since they do not block the upper regions (Resende et al., 2013, 2016). Thus, in these cases, we considered *fb*Es to be equal to *f*min, the minimum frequency of the upper layer trace seen in the ionogram. The Es_q and Es_b layers can be found in the analyzed regions since there is a displacement of the magnetic equator over the Brazilian sector. As mentioned before, the main difference between the Es_q and Es_b is their formation mechanism. The former is an irregularity layer due to the EEJ presence, whereas the latter is associated with the wind shear mechanism (Denardini et al., 2016; Resende et al., 2016).
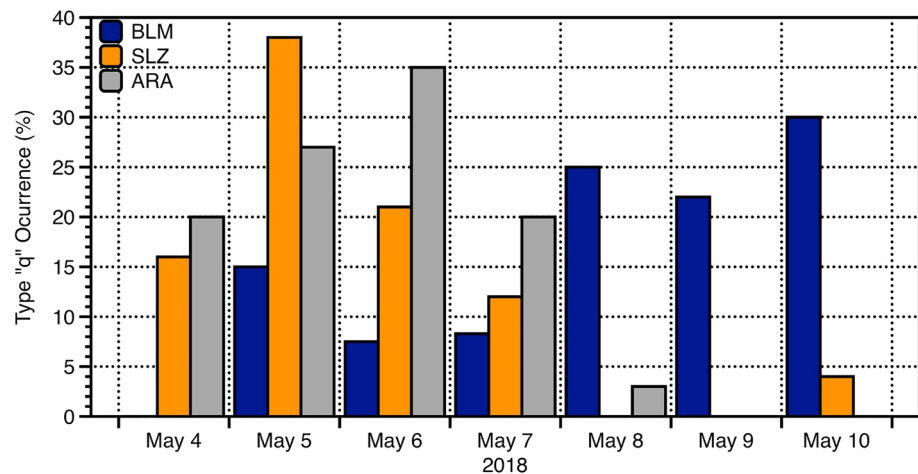
Figure 4. Daily values of percentage of the equatorial (Es$_q$) layer occurrence at Belém (BLM) (blue bar panels), São Luís (SLZ) (orange bar), and Araguatins (ARA) (gray bar) on May 04–10, 2018.

In Figure 3 the Es layer parameters are shown for both Es$_q$ and Es$_b$ types. Regarding the BLM station (Figure 3a), the Es layers were weak in general. During the periods of weak intensity, the amplitudes of the parameters ftEs and fbEs were comparable, not exceeding 5 MHz. It is important to mention here that, in equatorial regions, the fbEs is obtained when the F layer reflections begin ($f$minF). In this case, the lowest frequency in which an upper layer could be identified is adopted as the fbEs (Resende et al., 2013).

In SLZ (Figure 3b) and ARA (Figure 3c) stations, the fbEs daily variation presented a cosine-like behavior with maximum values of 5 MHz. We also observed some peaks in fbEs, the most prominent of them occurring during the recovery phase of the magnetic storm in SLZ, reaching 8 MHz at around 1800 UT on May 09. Furthermore, ftEs presented an oscillating behavior with values that reached three times the maximum fbEs values, that is, around 15 MHz in some hours, mainly over ARA. Also, the Es layer disappeared during a long period over SLZ between 1800 UT on May 07 and 0900 UT on May 08. Finally, concerning the ftEs in ARA, we noticed that the values were really high during all days of our analysis, surpassing 15 MHz most of the time and reaching 20 MHz at around the incidence of the HSS.

We computed the daily percentage of Es$_q$ layer occurrences for a more detailed assessment of this layer behavior using the ratio between the number of Es$_q$ layer observations and the total number of sounding measurements during the day. The results are presented in Figure 4, where the blue, orange, and gray bars correspond to the BLM, SLZ, and ARA regions, respectively. The ionograms of BLM on May 04 did not have an adequate resolution to be analyzed. Therefore, the daily Es$_q$ occurrence does not appear on this day. From this analysis, we conclude that the Es$_q$ occurred more frequently, relatively speaking, over SLZ and ARA during the magnetic storm main phase (May 05 and 06) than during the recovery phase. The occurrence in this phase was higher in SLZ (~38% on May 05), followed by ARA (35% on May 06), and BLM (16% on May 05). In the recovery phase, the Es$_q$ layer presence decreased significantly in the SLZ and ARA, not exceeding 20%. Additionally, the Es$_q$ layers disappeared during the magnetic storm recovery phase, between May 08 and 10 for SLZ and May 09 and 10 for ARA.

It is interesting the significant reduction of the equatorial Es$_q$ layer (<10%) over BLM on May 06 and 07, which is related to the EEJ low intensity. Rastogi (2006) studying the Indian sector found that the daytime EEJ is weakened during the magnetic storm main phase leading to Es$_q$ layer disruption that lasts even after the magnetic storm. The authors explained that this fact occurs due to a westward electric field imposed over the normal S_q field at the E region ionospheric heights, causing a CEJ event. These disturbed electric fields were provided by the disturbance dynamo electric field or prompt penetration electric field events.

We observed that the Es$_q$ layers reached higher values in BLM in the recovery phase (May 08, 09, and 10, 2018) than those we saw during the magnetic storm main phase (May 05 and 06). We believe that this behavior occurs because the magnetic equator is located near this region. Thus, the wind shear process is not so effective in BLM because the vertical component is almost null. Therefore, there is a strong condition
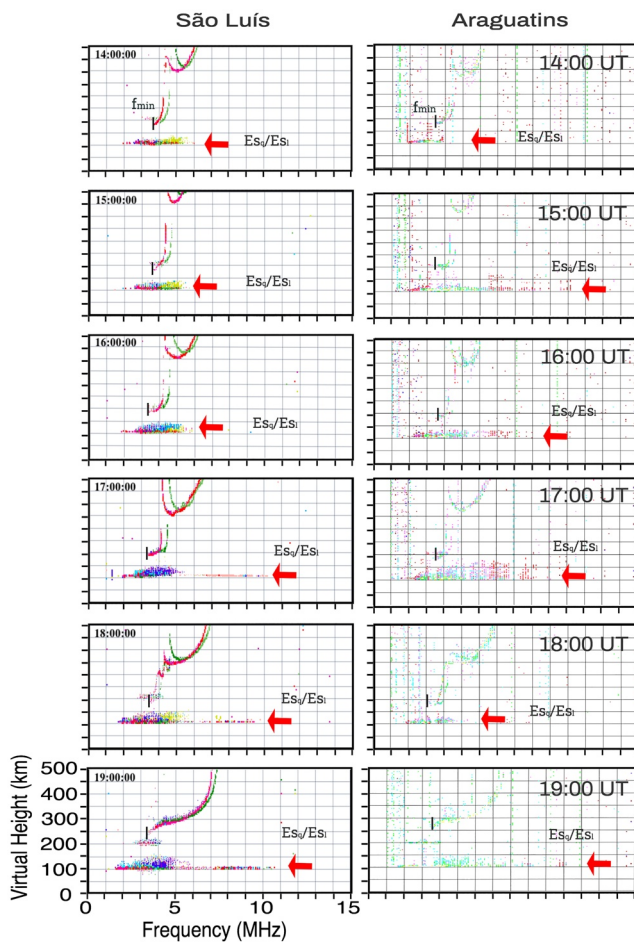
Figure 5. Ionograms collected at São Luís (SLZ) (left panel), and Araguatins (ARA) (right panel) from 1400 UT to 1900 UT on May 05, 2018, showing the equatorial (Es_q) and low (Es_l) layers.

(as the density gradient and polarization electric field) to develop a physical mechanism to form only the Es_q layers during daytime over BLM. This statement is supported by the observations conducted by Abdu et al. (1997) and Resende et al. (2013).

Some ionograms illustrating the Es layers (red arrows) are shown in Figure 5 on May 05, 2018. They include the period between 1400 UT and 1900 UT in increments of one hour for SLZ (left panel), and ARA (right panel). The Es_q layer was present in the three regions in conjunction with other Es layer types. In fact, the Es_l (low type) occurred in some hours for SLZ and ARA. This layer is a typical Es_b formed by the wind shear mechanism, which competes with the Es_q.

Furthermore, it is possible to notice that the lower frequency end of the F region minimum trace, represented by the $f$min (black line), was blocked after 1900 UT in both regions. Thus, we do not observe the entire F region trace in ionograms in this hour. This fact means the Es_b layer becomes more effective in these hours since the Es_q layer is transparent to radio waves (Resende et al., 2016).
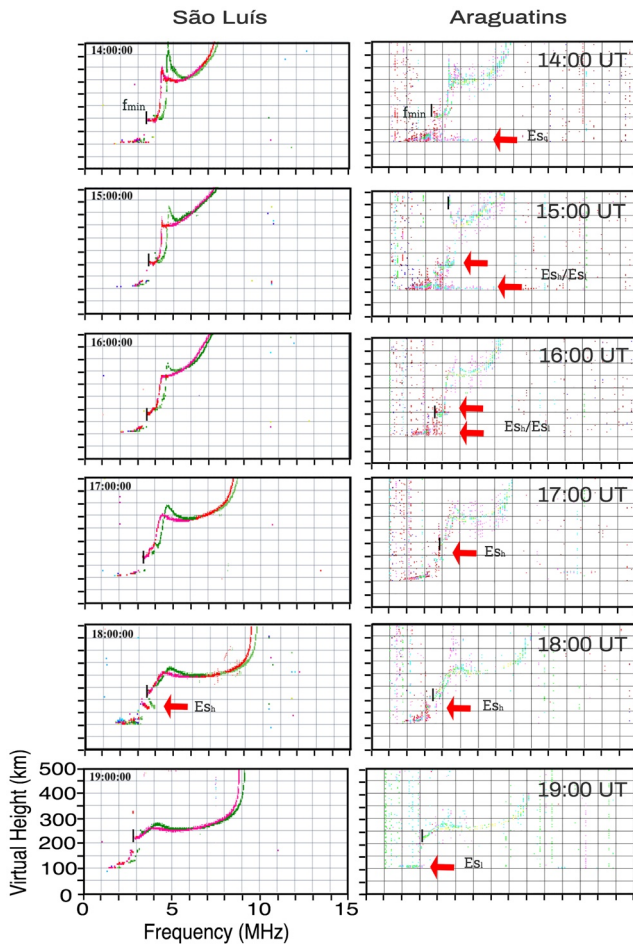
In this analysis, the Es_q layer over BLM is weak, not reaching values higher than 5 MHz (as shown in ionograms in the Figure S1). It is important to mention here that such behavior may have been caused by some technical problems of the BLM ionosonde, which can prevent the entire visualization of the Es_q layer. Thus, in BLM, the weak Es layer can indicate the equatorial Es layer presence. However, the Es_q layer is very weak or absent for the same period in another equatorial magnetic station, JIC (not shown here).

The simultaneous occurrence of both layers establishes two important facts: (a) the stations SLZ and ARA are still under the influence of the EEJ, even with the magnetic inclination angle higher than 7°, and (b) there is a competition between Es layer development mechanisms. Resende et al. (2016) analyzed the different Es layer characteristics in SLZ for 2005 and 2009. The authors were able to show the weakening of the EEJ instability, and the increasing role of the Es_b layers as the magnetic inclination increases. This fact occurred due to the apparent northwestward

movement of the geomagnetic equator over the Brazilian sector at a rate of ∼11.6′/year (∼21.7 km/year), as discussed before (Batista et al., 2011). Thus, the Es_b layers in SLZ were almost absent in 2005, whereas, in 2009, these layers occurred frequently. However, the Es_q layer did not entirely disappear from the ionograms collected in 2018.

This analysis shows that the winds and a weak EEJ influence are responsible for the Es layer formation in SLZ and ARA. Moreover, there is a possibility that the disturbance caused by the incidence of HSS can intensify this competition. In fact, Resende et al. (2013) analyzed the different Es layer types at a region near the magnetic equator during days around the magnetic storms in the solar cycle 23. They observed strong Es_q layers during the main phase of the magnetic storm. On the other hand, during the magnetic storm recovery phase, the EEJ current weakened, allowing the Es_b occurrence. Also, Denardini et al. (2016) found similar results, a weakening of the Es_q layer during the recovery phase of magnetic storms. Neither of the mentioned studies explains the Es_q strengthening/disruption during the magnetic storm phases.

The same behavior was observed on May 06, 2018 (not shown here), in which the Es_q and Es_b layer development mechanisms were competing at the stations analyzed. However, the Es_q layers are disrupted during the magnetic storm recovery phase in SLZ and ARA. Figure 6 shows the ionograms on May 08, 2018, for the same hour intervals as in Figure 5. The Es_q layer completely disappears in SLZ. Over ARA, the Es_q layer is very weak, and it is not possible to distinguish it from the other Es layer types (Es_b layers). Therefore, in these regions (SLZ and ARA), the tidal winds are dominant concerning the plasma irregularities. Even so,

Figure 6. Ionograms collected at São Luís (SLZ) (left panel), and Araguatins (ARA) (right panel) from 1400 UT to 1900 UT on May 08, 2018, showing the absence of the equatorial (Es$_q$) layer.

the Es$_b$ layers in these regions are not so intense since the wind amplitudes in equatorial sites are low (Resende et al., 2020). Thus, we have evidence that the strong and atypical Es layer (Es$_q$ layers) that occurred during the magnetic storm's main phase may be due to the intense electric field of the irregularities. Thus, we performed an investigation about the possible Es layer mechanism to explain this behavior.

3.3. The Influence of the EEJ in the Es Layer Development

Figure 7 presents the EEJ ground-strength variation on May 04–10, 2018, for (a) SLZ and (b) ARA during the disturbed (orange line) and quiet (green line) periods. The quiet period corresponds to the month's five international quiet day's average. As mentioned before, to evaluate the EEJ current, we used data from the quasi-equatorial site of our interest (SLZ, and ARA) and a station outside the magnetic equator (EUS). Although the values are not expressive, the results show that the variation pattern stills retain the EEJ characteristics from May 04 to May 06 in both regions but the amplitudes during daytime are higher than during the quiet periods, reaching almost 25 nT. After that, the EEJ current is less intense, having a similar behavior to that of periods without magnetic disturbances.

Therefore, the EEJ behavior of SLZ and ARA are very similar. The most remarkable intensification occurred on May 04, 2018. However, the Es$_q$ layer occurrence on this day was not as significant (~15% in SLZ and 20% in ARA in Figure 4) as in the magnetic storm main phase (~37% and ~27%). During this time period (the magnetic storm main phase time window is highlighted between dashed vertical lines in Figure 7), some evidence of magnetic disturbances appears in magnetometer data. We notice the fluctuations are comparable to those observed in the Bz (as shown in Figure 2). Also, this behavior is well related to the Es$_q$ layer presences in SLZ and ARA observed in Figure 4.

More recently, Moro et al. (2017) analyzed the Es layer occurrences over SLZ during the superstorm of November 2004. They found that the EEJ strength decreased significantly during the magnetic storm recovery phase, allowing the Es$_b$ layer formation. Even then, the electric fields were still intense enough to develop the Es$_q$ layers seen in ionograms in this phase. Thus, both Es layer types occurred in ionograms. This behavior was expected since the magnetic equator was closer to SLZ in 2004, as shown in Figure 1. It is possible that during the magnetic storm main phase, the disturbed electric fields in the E region plasma enlarged
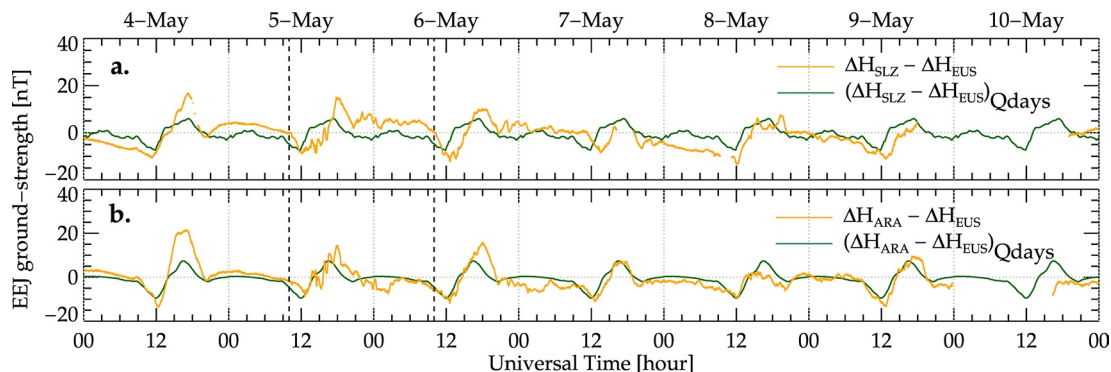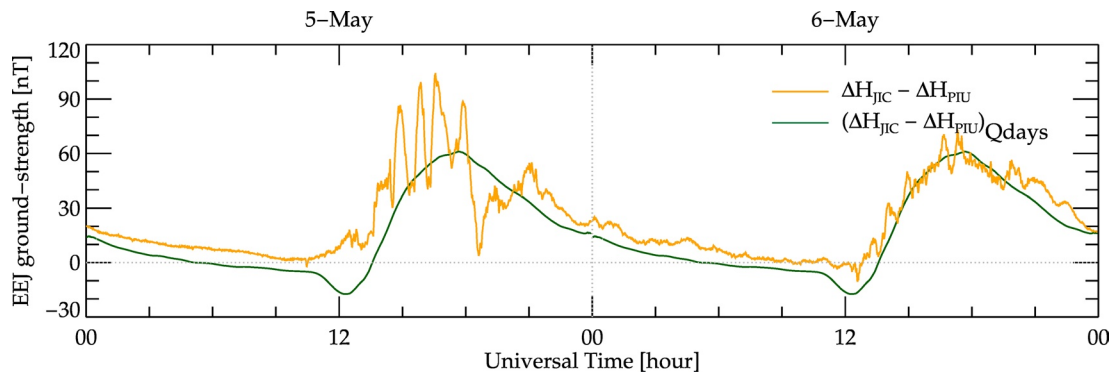

Figure 7. Temporal evolution of the Equatorial Electrojet (EEJ) ground strength using the magnetometer data from quasi-equatorial stations (São Luís [SLZ] and Araguatins [ARA]) and off equatorial station (EUS) on May 04–10, 2018.

Figure 8. Temporal evolution of the Equatorial Electrojet (EEJ) ground strength using the magnetometer data from Jicamarca (JIC), an equatorial station, and Piura (PIU), an off equatorial station on May 05 and 06, 2018. The orange line represents the disturbed periods, and the green line refers to the average of the four quietest days in May 2018.

the Gradient Drift instability structures as proposed by Devasia et al. (2006). These authors suggested that the disturbed electric field is associated with the large wind shears, forming Es_b and Es_q layers in regions located near the magnetic equator. In the present case the magnetic storm was caused by an HSS, not reaching significant SYM-H values. However, as mentioned before, the ΔH_{EEJ} for both regions presented a floating behavior on May 05, 2018, indicating a presence of the disturbed electric field, giving support to our hypothesis.

A significant enhancement in the EEJ intensity and the Gradient Drift instabilities were observed by Denardini et al. (2003) over SLZ during disturbed times in the years that the magnetic equator was very close to this region. They attributed this performance to the prompt penetration of an undershielding electric field, directed eastward in the diurnal period. Here, in our study, we have a challenge to study these disturbed electric fields since the E and F regions are like a close circuit in the ionosphere during the daytime (Abdu, 1997, Abdu et al., 2006).

To examine some disturbed ionospheric effect in the diurnal period, we used the magnetometer data from an equatorial region, Jicamarca, as proposed by Astafyeva et al. (2020). Figure 8 shows the ΔH_{EEJ} for disturbed periods on May 05 and 06 (orange line). The five quietest day's average was not calculated because of the fifth quiet day's data absence on May 26, 2018. Therefore, the green line in this figure refers to the four quietest day's average in May 2018. We used Piura as the off equatorial station to obtain the ΔH_{EEJ} (Equation 2). Notice that the EEJ ground-strength values are higher than in SLZ and ARA sites, reaching almost 100 nT. This fact is because the pair JIC-PIU measures the EEJ ground-strength at the EEJ center while the pairs SLZ-EUS and ARA-EUS are measuring at the EEJ border. Also, we observe strong fluctuations that can be a consequence of disturbed electric fields in this period. These electric fields can cause some intensification in the Gradient Drift instabilities during the daytime. As we expected, these fluctuations are observed with less intensity in the magnetometer data over SLZ and ARA since these regions are located at the border of the magnetic equator. However, these irregularities may have occurred in SLZ and ARA since the EEJ is slightly higher in disturbed periods than in the quiet days (Figure 6). This fact would justify the Es_q presence in these regions.

Additionally, as mentioned before, the Es_q layer has a decrease during the main phase of the magnetic storm in BLM (Figure 4), agreeing with the observation by Rastogi (2006) at other location and during another disturbed event. One hypothesis could be that the closer to the magnetic equator, the tidal wind role in the Es layer formation is almost ineffective since there is the absence of the horizontal component of the magnetic field, preventing a new layer formation. Therefore, we believe that the Es_q layer's continuous occurrence in BLM can be credit the EEJ behavior, even though this layer is weak. Unfortunately, we do not have any additional equipment, as coherent radar or magnetometers operational at BLM station to analyze this behavior with more details.

Finally, our results present evidence that there is a competition between the winds and electric fields during daytime in both SLZ and ARA stations. In this case study, the Gradient Drift instability may have been
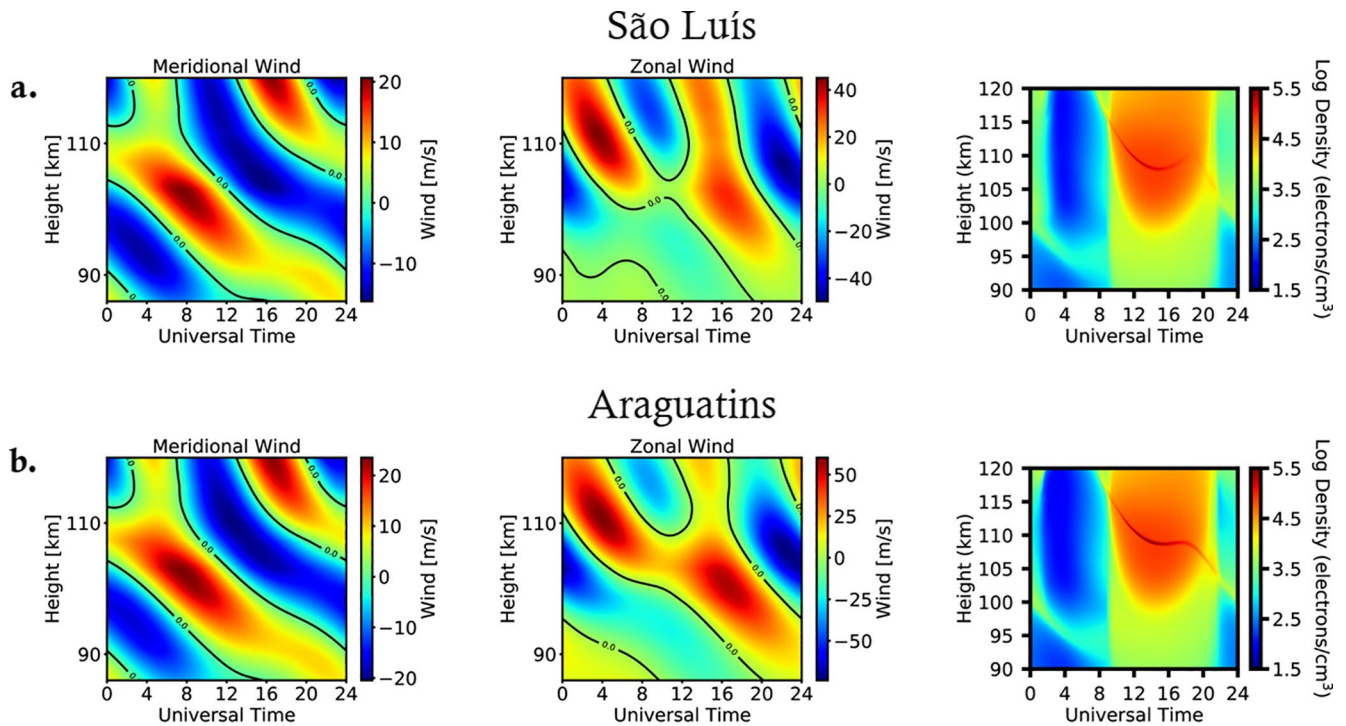
Figure 9. Wind profile of the meridional (left panel) and zonal (middle panel) components obtained using GSWM, and electron density (right panel) as a function of Universal Time (UT) and height (km) simulated by E Region Ionospheric Model (MIRE) considering the diurnal and semidiurnal tidal winds representative of May 2018 for (a) São Luís and (b) Araguatins.

effective during the disturbed periods in the SLZ and ARA, mainly during the magnetic storm main phase. Thus, the Es$_q$ layer can occur in some hours, even though these regions are believed to be located outside the influence of the EEJ. In the next section, we evaluate a possible effect of these disturbed electric fields in the Es layer formation using simulations.

### 3.4. The Es Layer Responses in MIRE Model

This work points out that the EEJ plasma irregularities can affect the Es layer development around the magnetic equatorial sites. The Es layer theory explains that the manifestation of the EEJ irregularity at the magnetic equator is present and, consequently, the Es$_q$ layer occurs frequently (Abdu et al., 1997; Resende et al., 2013). Also, in equatorial regions, the wind shear mechanism is not effective in forming sporadic E layers. Therefore, the Es$_b$ layer due to the windshear mechanism is not observed (Resende et al., 2016).

In the transition regions, as SLZ and ARA, we observe different Es layer formation mechanisms. The winds and electric fields driven by irregularities are competing in the Es layer development. To investigate this comportment, we used the MIRE model, which provides the Es layer density considering the winds and electric fields, already presented in Section 2.

Figure 9 shows the meridional (left panel) and the zonal (middle panel) wind components obtained using GSWM in May for SLZ (Figure 9a) and ARA (Figure 9b). The zero curves in the wind profiles refer to the wind shear mechanism responsible for the Es layer occurrence in simulations. Notice that the wind components show similar amplitudes at both locations, and that the zonal component amplitude is stronger than the meridional component, agreeing with the previous studies for other Brazilian regions (Resende et al., 2016, 2017b, 2020).

The electron density simulated by MIRE (Height-Time-Intensity maps) using the wind components mentioned above is presented in the right panel of Figure 9. The thin layers in the electron density maps refer to the Es$_b$ layers. The simulation background represents the regular E region, which is described by
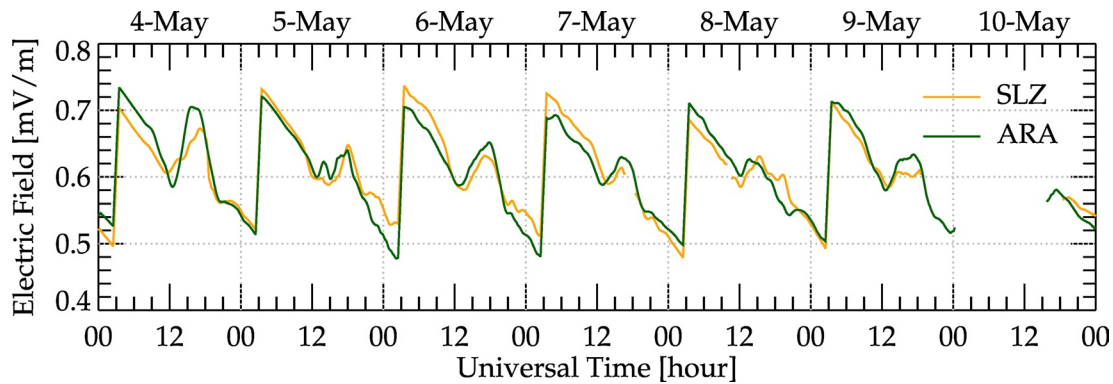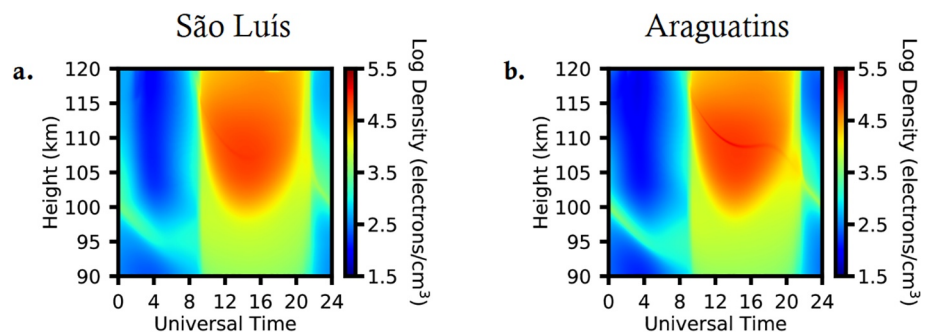
Figure 10. Zonal electric field profile on the May 04–10, 2018 in São Luís (SLZ) (orange line) and Araguatins (ARA) (green line).

the low (significant) electron density values in the nighttime (daytime). The Es_b layers present a common downward movement in observational data, due to the semidiurnal and diurnal tidal winds (Bishop & Earle, 2003; Haldoupis, 2011; Haldoupis et al., 2006; Pignalberi et al., 2014, 2015; Santos et al., 2019). In SLZ, the Es_b layer formed around 120 km and descended to approximately 107 km between 0800 and 1500 UT. Similar behavior is seen in ARA, in which the Es_b layer descends until it reaches approximately 107 km at around 1500 UT. After that, the Es_b layer has an abrupt rise in both regions but then returning its descent behavior. Another important characteristic observed is that the electron density of the Es_b layers has smaller values during the nighttime. All these features are typical of the Es layer formed by winds, as discussed in Resende et al. (2017a).

In this study, the Gradient Drift instability's electric field was obtained through the methodology developed by Anderson et al. (2004). We included the ΔH measurements (Figure 7) in Equation 6 to get the vertical drift velocity ($E \times B/B^2$). Thus, we obtain the zonal electric field using the relationship that a variation of 40 m/s in the vertical drift velocity equals 1 mV/m, as proposed in Fejer and Scherliess (1995). The results for the zonal electric profile of the EEJ are shown in Figure 10 for SLZ (orange line), and ARA (green line) on May 04–10, 2018. In general, the electric field values in these regions did not reach 0.75 mV/m, agreeing with the previous study in equatorial regions (Moro et al., 2017; Resende et al., 2016). During the magnetic storm main phase (around 1000 UT on May 06), we notice an enhancement in the electric field in SLZ. However, we do not observe significant changes in this component for ARA.

Therefore, the eastward zonal electric field was included in MIRE to analyze their effect on the Es_b layer formation or disruption. Here, we decided to include the electric field values during the main phase of the magnetic storm (May 05) in the daytime, which is when the Es_q layer occurs in the ionograms. The HTI maps are shown in Figure 11 for (a) SLZ and (b) ARA. In both regions the intensity of the Es layers reduces significantly. Comparing these results with the simulations using only the winds (Figure 8), the Es_b layer density decreased around 51% and 62% during the daytime, at SLZ, and ARA, respectively. In SLZ, at certain

Figure 11. Electron density simulated by E Region Ionospheric Model considering the winds and the zonal electric field profiles on May 05, 2018 in (a) São Luís, and (b) Araguatins.

times of the day, the Es layer's electron density is similar to the background density, making it difficult to observe this layer. Thus, in this study, the Es_b layer did not disappear completely, unlike the results seen in Moro et al. (2017). Notice that the EEJ mechanism is not considered in MIRE, and, therefore, the Es_q layer cannot be simulated. Therefore, an eastward electric field in the simulations causes a weakening in the Es_b layer development. This electric field component can be intensified during these disturbed times and may have strengthened the EEJ irregularities.

This equatorial Es layer behavior was discussed in some works as Reddy and Devasia (1973) and Resende et al. (2016), in which they affirm that the plasma irregularities in this region can inhibit the Es_b layer development. In our simulations, the eastward zonal electric field is not strong enough to disrupt the Es_b layer but is able to cause its significant modification. This behavior is seen in ionograms, in which the Es_b layers do not block the F region until 1800 UT for BLM, ARA, and SLZ. Therefore, the disturbed electric field weakens the Es_b layers, and at the same time, allows the EEJ plasma instabilities to grow in the E region plasma. This relationship between the Es_b layer weakening and the eastward electric field is confirmed in our simulations.

Thus, we believe that the presence of Es_q over SLZ and ARA is a concrete evidence of the EEJ influence during the May 05 and 06, 2018 magnetic storm's main phase. There is a high possibility that the Gradient Drift instability excitation associated with a large electron density gradient, and a strong eastward electric field in this period was the Es_q layer precursor (Moro et al., 2017). Our results confirm that the EEJ can still influence the regions located on the border of the magnetic equator. In fact, this study reveals that the EEJ may cause some influence in regions until the magnetic inclination around 11°, disagreeing with the previous works that mention that its effect is up to 7° (Forbes, 1981; Moro et al., 2017; Resende et al., 2016).

Last, in the region very close to the magnetic equator as BLM, the wind shear is not effective, inhibiting the Es_b formation (Whitehead, 1961). The low occurrence of the Es_q layer in the period studied (Figure 4) may be due to the density gradient was not so strong in this period. This fact will require a future investigation with more available data.

4. Conclusions

We presented a study about the Es layer dynamics during a high-speed solar wind stream event on May 05 and 06, 2018, in the Brazilian sector. We analyzed the ionosonde data, magnetometer data, and modeling results to obtain Es layer formation responses over regions located in the magnetic equator border (SLZ and ARA).

In this study, the Es_q layer occurrence is related to the Gradient Drift instability of the EEJ, whereas the other Es layer types (Es_b) occur due to the tidal winds through the wind shear mechanism. We observed that both Es_q and Es_b layers develop simultaneously during the magnetic storm main phase in the boundary equatorial magnetic sites, SLZ and ARA. Thus, we deeply investigated the EEJ effect considering its physical dynamics. In this period, the magnetometer data showed positive amplitudes higher than the quiet periods and strong fluctuations that can be a consequence of disturbed electric field, meaning an eastward electric field occurrence. Although the amplitudes are observed with less intensity in the magnetometer data over SLZ and ARA concerning the Peruvian sector, it is clear that the eastward disturbed electric field is acting in this period. Thus, these electric fields can cause some intensification in the Gradient Drift instabilities. Hence, we show that Gradient Drift instability can intensify during disturbed periods during the daytime, extending the EEJ influence to these border regions. Therefore, this work reveals that the EEJ may influence areas up to 11° of magnetic inclination.

We analyzed a region located precisely in the magnetic equatorial line (BLM). The Es_b layer due to the wind shear is not formed in this station. On the other hand, the Es_q layer in the studied period was weak in this region. The same behavior was seen in JIC, in which the Es_q layer was very weak or absent for the same period. However, as we have some technical problems with the BLM ionosonde, which can prevent the entire visualization of the Es_q layer, this behavior requires further investigation with more data to be fully understood.

Furthermore, our investigation was carried out using a simulation from MIRE. It was possible to calculate the eastward zonal electric field in the disturbed period using the relationship between the magnetic field

H component and the vertical drift velocity. In this case, the electric field is enough to weaken the Es_b layer seen in the modeling results. This electric field component can be intensified during these disturbed times and may have strengthened the EEJ irregularities. Therefore, we prove that the EEJ influence expands beyond the expected boundaries during disturbed periods, causing Es_q layers in SLZ and ARA, which are expected to be low latitude regions due to the magnetic equator drift. Finally, the EEJ influence expansion dynamics was modeled inside MIRE for the first time, and the simulation results corroborated our observational data.

Data Availability Statement

The magnetometer data from São Luís, Araguatins, and Eusébio, and Digisonde data from Belém and São Luís can be downloaded upon registration at the Embrace webpage from INPE Space Weather Program in the following link: http://www2.inpe.br/climaespacial/portal/en/.

References

Abdu, M. A. (1997). Major phenomena of the equatorial ionosphere-thermosphere system under disturbed conditions. *Journal of Atmospheric and Terrestrial Physics*, *59*, 1505–1519. https://doi.org/10.1016/S1364-6826(96)00152-6

Abdu, M. A., & Batista, I. S. (1977). Sporadic E-layer phenomena in the Brazilian geomagnetic anomaly: Evidence for a regular particle ionization source. *Journal of Atmospheric and Terrestrial Physics*, *39*(6), 723–732. https://doi.org/10.1016/0021-9169(77)90059-9

Abdu, M. A., Batista, I. S., MacDougall, J., Sobral, J. H. A., & Muralikrishna, P. (1997). Permanent changes in sporadic E layers over Fortaleza, Brazil. *Advances in Space Research*, *20*(11), 2165–2168. https://doi.org/10.1016/S0273-1177(97)00610-8

Abdu, M. A., de Souza, J. R., Sobral, J. H. A., & Batista, I. S. (2006). Magnetic storm associated disturbance dynamo effects in the low and equatorial latitude ionosphere, in recurrent magnetic storms: Corotating solar wind streams. *Geophysical Monograph Series*, *167*, 283–304. https://doi.org/10.1029/167GM22

Anderson, D., Anghel, A., Chau, J., & Veliz, O. (2004). Daytime vertical E × B drift velocities inferred from ground-based magnetometer observations at low latitudes. *Space Weather*, *2*, S11001. https://doi.org/10.1029/2004SW000095

Astafyeva, E., Bagiya, M. S., Förster, M., & Nishitani, N. (2020). Unprecedented hemispheric asymmetries during a surprise ionospheric storm: A game of drivers. *Journal of Geophysical Research: Space Physics*, *125*, e2019JA027261. https://doi.org/10.1029/2019JA027261

Batista, I. S., Diogo, E. M., Souza, J. R., Abdu, M. A., & Bailey, G. J. (2011). Equatorial ionization anomaly: The role of thermospheric winds and the effects of the geomagnetic field secular variation. In M. A. Abdu, & D. Pancheva (Eds.), *Aeronomy of the Earth's atmosphere and ionosphere* (pp. 317–328). Dordrecht: Springer. https://doi.org/10.1007/978-94-007-0326-1_23

Bishop, R. L., & Earcle, G. D. (2003). Metallic ion transport associated with midlatitude intermediate layer development. *Journal of Geophysical Research*, *108*(A1), 10–19. https://doi.org/10.1029/2002JA009411

Buriti, R. A., Hocking, W. K., Batista, I. S., & Medeiros, A. F. (2008). Observations of equatorial mesospheric winds over Cariri (7.4°S) by a meteor radar and comparison with existing models. *Annales Geophysicae*, *26*, 485–497. https://doi.org/10.5194/angeo-26-485-2008

Carrasco, A. J., Batista, I. S., & Abdu, M. A. (2007). Simulation of the sporadic E layer response to pre-reversal associated evening vertical electric field enhancement near dip equator. *Journal of Geophysical Research*, *112*(A06), 324–335. https://doi.org/10.1029/2006JA012143

Da Silva, L. A., Shi, J., Alves, L. R., Sibeck, D., Souza, V. M., Marchezi, J. P., et al. (2021). Dynamic mechanisms associated with high-energy electron flux dropout in the Earth's outer radiation belt under the influence of a coronal mass ejection sheath region. *Journal of Geophysical Research: Space Physics*, *126*, e2020JA028492. https://doi.org/10.1029/2020JA028492

Da Silva, L. A., Sibeck, D., Alves, L. R., Souza, V. M., Jauer, P. R., Claudepierre, S. G., et al. (2019). Contribution of ULF wave activity to the global recovery of the outer radiation belt during the passage of a high-speed solar wind stream observed in September 2014. *Journal of Geophysical Research: Space Physics*, *124*, 1660–1678. https://doi.org/10.1029/2018JA026184

Denardini, C. M., Abdu, M. A., Aveiro, H. C., Resende, L. C. A., Almeida, P. D. S. C., Olivio, E. P. A., et al. (2009). Counter electrojet features in the Brazilian sector: Simultaneous observation by radar, digital sounder and magnetometers. *Annales Geophysicae*, *27*, 1593–1603. https://doi.org/10.5194/angeo-27-1593-2009

Denardini, C. M., Abdu, M. A., De Paula, E. R., Sobral, J. H. A., & Wrasse, C. M. (2005). Seasonal characterization of the equatorial electrojet height rise over Brazil as observed by the RESCO 50 MHz back-scatter radar. *Journal of Atmospheric and Terrestrial Physics*, *67*, 1665–1673. https://doi.org/10.1016/j.jastp.2005.04.008

Denardini, C. M., Abdu, M. A., & Sobral, J. H. A. (2003). Detection of three distinct regions in the equatorial electrojet in the Brazilian sector. *Brazilian Journal Geophysics*, *21*(1), 65–74. https://doi.org/10.1590/S0102-261X2003000100006

Denardini, C. M., Abdu, M. A., & Sobral, J. H. A. (2004). VHF radar studies of the equatorial electrojet 3-m irregularities over São Luís: Day-to-day variabilities under auroral activity and quiet conditions. *Journal of Atmospheric and Terrestrial Physics*, *66*(17), 1603–1613. https://doi.org/10.1016/j.jastp.2004.07.031

Denardini, C. M., Chen, S. S., Resende, L. C. A., Moro, J., Bilibio, A. V., Fagundes, P. R., et al. (2018). The embrace magnetometer network for South America: Network description and its qualification. *Radio Science*, *53*, 288–302. https://doi.org/10.1002/2017RS006477

Denardini, C. M., Resende, L. C. A., Moro, J., & Chen, S. S. (2016). Occurrence of the blanketing sporadic E layer during the recovery phase of the October 2003 superstorm. *Earth Planets and Space*, *68*(80), 1–9. https://doi.org/10.1186/s40623-016-0456-7

Devasia, C. V., Jyoti, N., Subbarao, K. S. V., Tiwari, D., Reddi, C. R., & Sridharan, R. (2004). On the role of vertical electron density gradients in the generation of type II irregularities associated with blanketing Es (Es_b) during counter equatorial electrojet events: A case study. *Radio Science*, *39*, RS3007. https://doi.org/10.1029/2002RS002725

Devasia, C. V., Sreeja, V., & Ravindran, S. (2006). Solar cycle dependent characteristics of the equatorial blanketing Es layers and associated irregularities. *Annales Geophysicae*, *24*(11), 2931–2947. https://doi.org/10.5194/angeo-24-2931-2006

Fejer, B. G., & Scherliess, L. (1995). Time dependent response of equatorial ionospheric electric fields to magnetospheric disturbances. *Geophysical Research Letters*, *22*, 851–854. https://doi.org/10.1029/95gl00390

Forbes, J. M. (1981). The equatorial electrojet. *Reviews of Geophysics*, *19*(3), 469–504. https://doi.org/10.1029/RG019i003p00469

Gonzalez, W. D., Joselyn, J. A., Kamide, Y., Kroehl, H. W., Rostoker, G., Tsurutani, B. T., & Vasyliunas, V. M. (1994). What is a magnetic storm? *Journal of Geophysical Research*, *99*(A4), 5771–5792. https://doi.org/10.1029/93JA02867

Hagan, M. E., & Forbes, J. M. (2002). Migrating and nonmigrating diurnal tides in the middle and upper atmosphere excited by tropospheric latent heat release. *Journal of Geophysical Research*, *107*, 4754. https://doi.org/10.1029/2001JD001236

Hagan, M. E., & Forbes, J. M. (2003). Migrating and nonmigrating semidiurnal tides in the upper atmosphere excited by tropospheric latent heat release. *Journal of Geophysical Research*, *108*, 1062. https://doi.org/10.1029/2002JA009466

Hajra, R., Tsurutani, B. T., Brum, C. G. M., & Echer, E. (2017). High-speed solar wind stream effects on the topside ionosphere over Arecibo: A case study during solar minimum. *Geophysical Research Letters*, *44*, 7607–7617. https://doi.org/10.1002/2017GL073805

Haldoupis, C. (2011). A tutorial review on sporadic E layers. Aeronomy of the Earth's atmosphere-ionosphere. In *IAGA Book Series* (Vol. 2, pp. 381–394). https://doi.org/10.1007/978-94-007-0326-1_29

Haldoupis, C., Meek, C., Christakis, N., Pancheva, D., & Bourdillon, A. (2006). Ionogram height-time intensity observations of descending sporadic E layers at mid-latitude. *Journal of Atmospheric and Terrestrial Physics*, *68*(539), 539–557. https://doi.org/10.1016/j.jastp.2005.03.020

Knecht, R. W., & McDuffie, R. E. (1962). In E. K. Smith, & S. Matsushita (Eds.), *On the width of the equatorial Es belt, Ionospheric sporadic E* (pp. 215–218). New York: Pergamon Press. https://doi.org/10.1016/B978-0-08-009744-2.50022-9

Kopp, E. (1997). On the abundance of metal ions in the lower ionosphere. *Journal of Geophysical Research*, *102*, 9667–9674. https://doi.org/10.1029/97JA00384

MacDougall, J. W., Grant, I. F., & Shen, X. (1995). *The Canadian advanced digital ionosonde: Design and results, report UAG-14: Ionospheric networks and stations* (pp. 21–27). World Data Center A for Solar-Terrestrial Physics.

Mathews, J. D. (1998). Sporadic E: Current views and recent progress. *Journal of Atmospheric and Terrestrial Physics*, *60*, 413–435. https://doi.org/10.1016/S1364-6826(97)00043-6

Moro, J., Denardini, C. M., Resende, L. C. A., Chen, S. S., & Schuch, N. J. (2016a). Equatorial E-region electric fields at the dip equator-I. Variabilities in eastern Brazil and Peru. *Journal of Geophysical Research: Space Physics*, *121*, 10220–10230. https://doi.org/10.1002/2016JA022751

Moro, J., Denardini, C. M., Resende, L. C. A., Chen, S. S., & Schuch, N. J. (2016b). Equatorial E-region electric fields at the dip equator-II. Seasonal variabilities and effects over Brazil due to the secular variation of the magnetic equator. *Journal of Geophysical Research: Space Physics*, *121*, 10231–10240. https://doi.org/10.1002/2016JA022753

Moro, J., Resende, L. C. A., Denardini, C. M., Xu, J., Batista, I. S., Andrioli, V. F., & Schuch, N. J. (2017). Equatorial E region electric fields and sporadic E layer responses to the recovery phase of the November 2004 geomagnetic storm. *Journal of Geophysical Research: Space Physics*, *122*, 12517–12533. https://doi.org/10.1002/2017JA024734

Nogueira, P. A. B., Abdu, M. A., Souza, J. R., Bailey, G. J., Batista, I. S., Shume, E. B., & Denardini, C. M. (2013). Longitudinal variation in global navigation satellite systems TEC and topside ion density over South American sector associated with the four-peaked wave structures. *Journal of Geophysical Research: Space Physics*, *118*, 7940–7953. https://doi.org/10.1002/2013JA019266

Piggott, W., & Rawer, K. (1972). *Handbook of ionogram interpretation and reduction* (pp. 352). US Department of Commerce.

Pignalberi, A., Pezzopane, M., & Zuccheretti, E. (2014). Sporadic E layer at mid-latitudes: Average properties and influence of atmospheric tides. *Annales Geophysicae*, *32*, 1427–1440. https://doi.org/10.5194/angeo-32-1427-201

Pignalberi, A., Pezzopane, M., & Zuccheretti, E. (2015). A spectral study of the mid-latitude sporadic E layer characteristic oscillations comparable to those of the tidal and the planetary waves. *Journal of Atmospheric and Terrestrial Physics*, *122*, 34–44. https://doi.org/10.1016/j.jastp.2014.10.017

Pillat, V. G., Guimarães, L. N. F., Fagundes, P. R., & Silva, J. D. S. (2013). A computational tool for ionosonde CADI's ionogram analysis. *Computers and Geosciences*, *52*, 372–378. https://doi.org/10.1016/j.cageo.2012.11.009

Ponomarev, E. A., Sedykh, P. A., & Urbanovich, V. D. (2006). Bow shock as a power source for magnetospheric processes. *Journal of Atmospheric and Terrestrial Physics*, *68*, 685–690. https://doi.org/10.1016/j.jastp.2005.11.007

Rastogi, R. G. (1972). Equatorial sporadic E and plasma instabilities. *Nature*, *237*, 73. https://doi.org/10.1038/237073a0

Rastogi, R. G. (1997). Midday reversal of equatorial ionospheric electric field. *Annales Geophysicae*, *15*, 1309–1315. https://doi.org/10.1007/s00585-997-1309-2

Rastogi, R. G. (2006). Magnetic storm effects at equatorial electrojet stations. *Earth Planets and Space*, *58*(5), 645–657. https://doi.org/10.1186/BF03351962

Reddy, C. A., & Devasia, C. V. (1973). Formation of blanketing sporadic E layers at the magnetic equator due to horizontal wind shears. *Planet Space Science*, *21*(5), 811–817. https://doi.org/10.1016/0032-0633(73)90098-6

Reinisch, B. W., Galkin, I. A., Khmyrov, G. M., Kozlov, A. V., Bibl, K., Lisysyan, I. A., et al. (2009). New digisonde for research and monitoring applications. *Radio Science*, *44*, RS0A24. https://doi.org/10.1029/2008RS004115

Reinisch, B. W., & Huang, X. (1983). Automatic calculation of electron density profiles from digital ionograms: 3. Processing of bottom side ionograms. *Radio Science*, *18*(3), 477–492. https://doi.org/10.1029/RS018i003p00477

Resende, L. C. A., Batista, I. S., Denardini, C. M., Batista, P. P., Carrasco, A. J., Andrioli, V. F., & Moro, J. (2017a). Simulations of blanketing sporadic E-layer over the Brazilian sector driven by tidal winds. *Journal of Atmospheric and Solar-Terrestrial Physics*, *154*, 104–114. https://doi.org/10.1016/j.jastp.2016.12.012

Resende, L. C. A., Batista, I. S., Denardini, C. M., Batista, P. P., Carrasco, J. A., Andrioli, V. F., & Moro, J. (2017b). The influence of tidal winds in the formation of blanketing sporadic E-layer over equatorial Brazilian region. *Journal of Atmospheric and Solar-Terrestrial Physics*, *171*, 64–67. https://doi.org/10.1016/j.jastp.2017.06.009

Resende, L. C. A., Batista, I. S., Denardini, C. M., Carrasco, A. J., Andrioli, V. F., Moro, J., et al. (2016). Competition between winds and electric fields in the formation of blanketing sporadic E layers at equatorial regions. *Earth Planets and Space*, *68*, 201. https://doi.org/10.1186/s40623-016-0577-z

Resende, L. C. A., Denardini, C. M., & Batista, I. S. (2013). Abnormal *fb*Es enhancements in equatorial Es layers during magnetic storms of solar cycle 23. *Journal of Atmospheric and Terrestrial Physics*, *102*, 228–234. https://doi.org/10.1016/j.jastp.2013.05.020

Resende, L. C. A., Shi, J., Denardini, C. M., Batista, I. S., Nogueira, P. A. B., Arras, C., et al. (2020). The influence of disturbance dynamo electric field in the formation of strong sporadic E layers over Boa Vista, a low-latitude station in the American sector. *Journal of Geophysical Research: Space Physics*, *125*, e2019JA027519. https://doi.org/10.1029/2019JA027519

Resende, L. C. A., Shi, J., Denardini, C. M., Batista, I. S., Picanço, G. A., Moro, J., et al. (2021). The impact of the disturbed electric field in the sporadic E (Es) layer development over Brazilian region. *Journal of Geophysical Research: Space Physics*, *126*, e2020JA028598. https://doi.org/10.1029/2020JA028598

Rout, D., Chakrabarty, D., Janardhan, P., Sekar, R., Maniya, V., & Pandey, K. (2017). Solar wind flow angle and geoeffectiveness of corotating interaction regions: First results. *Geophysical Research Letters*, *44*, 4532–4539. https://doi.org/10.1002/2017GL073038

Santos, A. M., Batista, I. S., Abdu, M. A., Sobral, J. H., Souza, J. R., & Brum, C. G. M. (2019). Climatology of intermediate descending layers (or 150 km echoes) over the equatorial and low-latitude regions of Brazil during the deep solar minimum of 2009. *Annales Geophysicae*, *37*, 1005–1024. https://doi.org/10.5194/angeo-37-1005-2019

Shue, J. H., Song, P., Russell, C. T., Steinberg, J. T., Chao, J. K., Zastenker, G., et al. (1998). Magnetopause location under extremes solar wind conditions. *Journal of Geophysical Research*, *103*(17), 691–697. https://doi.org/10.1029/98JA01103

Stone, E. C., Frandsen, A. M., Mewaldt, R. A., Christian, E. R., Margolies, D., Ormes, J. F., & Snow, F. (1998). The advanced composition explorer. *Space Science Reviews*, *86*(1–4), 1–22. https://doi.org/10.1023/A:1005082526237

Tsurutani, B. T., Gonzalez, W. D., Gonzalez, A. L., Tang, F., Arballo, J. K., & Okada, M. (1995). Interplanetary origin of geomagnetic activity in the declining phase of the solar cycle. *Journal of Geophysical Research*, *100*(A11), 717–733. https://doi.org/10.1029/95JA01476

Whitehead, J. (1961). The formation of the sporadic-E in the temperate zones. *Journal of Atmospheric and Terrestrial Physics*, *20*(1), 1155–1167. https://doi.org/10.1016/0021-9169(61)90097-6

Whitehead, J. D. (1989). Recent work on mid-latitude and equatorial sporadic-E. *Journal of Atmospheric and Terrestrial Physics*, *51*(5), 401–424. https://doi.org/10.1016/0021-9169(89)90122-0